Far-infrared surface-Landau-level spectroscopy in Bi

M. Wanner and R. E. Doezema
Physik-Department, Technische Universität München, 8046 Garching, Germany

U. Strom
Naval Research Laboratory, Washington, D.C. 20375

(Received 17 April 1975)

Surface-Landau-level resonance data in Bi are presented at four far-infrared frequencies: 890.7, 1362.5, 1747.1, and 2526.6 GHz. The magnetic field positions of the resonances compare well with the predictions of a semiclassical calculation which takes into account the deviation from the well-established theory for the surface-state resonances valid at microwave frequencies. These deviations occur in the far-infrared primarily because the excitation energy $\hbar\omega$ becomes comparable to the Bi Fermi energy. We incorporate nonparabolic effects into the semiclassical calculation by using the two-band model to describe surface Landau levels in the nonparabolic conduction band of Bi. The influence of the far-infrared effects on line shape is discussed together with the lack of observable surface-roughness scattering.

I. INTRODUCTION

Surface-Landau-level resonance[1] at microwave frequencies has proved to be a powerful method for determining electron velocities and thermal scattering rates point by point on the Fermi surfaces of metals and semimetals.[2] Because the usual condition $\omega\tau > 1$ on the frequency ω and relaxation time τ must be satisfied, it would appear that the extension of such studies to higher frequencies is desirable, and might be especially helpful, for example, in investigating anisotropic scattering rates in alloy systems. Furthermore, the frequency dependence of τ, which becomes important at higher frequencies, could be investigated as a function of Fermi-surface location.

Aside from the very important experimental considerations of sample-surface preparation, which becomes ever more crucial with increasing frequency, it is necessary to examine to which extent the theoretical assumptions valid in the microwave regime hold at higher frequencies. To explore such aspects, the semimetal Bi turns out to be an ideal candidate. The surface-state resonances in Bi have been studied in great detail at microwave frequencies[3,4]; here, we report the extension to the far infrared. We begin by reviewing the main features of surface-state resonance in the microwave regime.

The surface level is simply an electron state bound to the surface by the magnetic force $-(e/c)\vec{v}_F\times\vec{H}$. The magnetic field H is applied parallel to the sample surface. At microwave frequencies, the surface state corresponds classically to an electron moving in a very shallow skipping orbit along the surface with Fermi velocity v_F (Fig. 1). The orbit is so shallow that the magnetic force $(e/c)v_FH$ is essentially directed normal to the sample surface, and the resulting potential increases linearly into the sample, $V=(e/c)v_FHz$. The electron is therefore trapped in the potential well formed by this linear potential and the surface potential, taken to be infinite. The energy levels in this well can be easily calculated by a semiclassical approach,[4] and are found to be in close agreement with those obtained from the rigorous theory.[1]

A. Semiclassical calculation for microwaves

The semiclassical calculation proceeds as follows. Using the Bohr-Sommerfeld rule, we require for the periodic z-directed momentum

$$\oint p_z\,dz = 2\int_0^{z_n} p_z\,dz = (n-\tfrac{1}{4})h\,. \tag{1}$$

Here, n is a positive integer, and the phase factor $\frac{1}{4}$ is appropriate for the case of a simple linear turning point of the motion. Evaluation of the integral for the shallow-orbit case leads to an expression for the maximal depth of penetration,

$$z_n = (ch/e)^{1/3}\,(\tfrac{3}{4}\pi^{1/2}\,(n-\tfrac{1}{4}))^{2/3}\,(HK)^{-1/3}\,. \tag{2}$$

We are for simplicity (and because of its applicability to Bi) considering a cylindrical Fermi surface of radius K whose axis is along the H direction. The classical turning point is defined by $E_n = (e/c)v_FHz_n$; hence, the energy levels are given by

$$E_n = (e^2h/c^2)^{1/3}\,H^{2/3}\,(v_F^3/K)^{1/3}\,[\tfrac{3}{4}\pi^{1/2}\,(n-\tfrac{1}{4})]^{2/3}\,. \tag{3}$$

By requiring

$$E_n - E_m = \hbar\omega\,, \tag{4}$$

one obtains from Eq. (3) the resonance fields at frequency ω:

$$H_{mn} = \frac{c\hbar}{e}\left(\frac{\omega}{a_n-a_m}\right)^{3/2}\left(\frac{2K}{v_F^3}\right)_\perp^{1/2}\,. \tag{5}$$

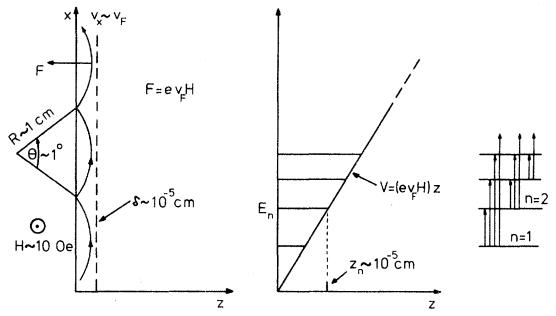

FIG. 1. Electron skipping trajectory and corresponding potential well for a free-electron metal in the microwave regime.

We have included here the symbol $\perp$ to indicate that, for a general Fermi surface, both K and v_F are to be taken in the plane perpendicular to $\vec{H}$. In this expression, $a_n = [(3\pi/2)(n - \frac{1}{4})]^{2/3}$. The energy levels of Eq. (3) differ by only about 1% from those of the rigorous theory for the low-lying levels, and agreement improves with increasing n.

For a typical metal at frequency ~ 30 GHz, one finds $H_{mn} \sim 10$ Oe for the low-level transitions, also in this field range $z_n \sim 10^{-5}$ cm (comparable to the skin layer δ). The cyclotron radius $R\,(= c\hbar K/eH)$ is ~1 cm, however, so that the orbits are indeed very shallow and the skipping electron is localized to nearly a point on the Fermi surface with parameters K and v_F.

B. High-frequency considerations

At microwave frequencies, the level spacing $\hbar\omega$ is very small compared to the Fermi energy E_F; therefore, for $T \sim 4\,^\circ$K one has

$$\hbar\omega \lesssim k_B T \ll E_F \tag{6}$$

($\hbar\omega \sim 1$ K, and for Bi, $E_F \sim 300$ K). The microwave photons impart no momentum parallel to the surface, so that for a given transition, the momentum component p_x parallel to the surface is conserved. The transition, of course, must take place within about $k_B T$ of the Fermi energy; this means that the allowed p_x values have a spread about p_F of

$$\Delta p_x / p_F \approx k_B T / E_F \ll 1 . \tag{7}$$

The energy differences $E_n - E_m$ are, as a result (for small m, n), essentially independent of p_x, and the allowed transitions take place within the manifold of p_x values at energy[5] $\hbar\omega$. This situation is illustrated in Fig. 2.

Raising the frequency sufficiently causes Eq. (6) to be replaced by

$$k_B T \ll \hbar\omega \lesssim E_F . \tag{8}$$

This condition, which in Bi is attained in the far infrared, has a number of consequences.

1. p_x broadening

The energy states which participate in the transitions fall in the range $E_F \pm \hbar\omega$, i.e., from deep inside the Fermi sea to far above it. One can no longer neglect the p_x dependence of the energy differences $E_n - E_m$, because the spread in p_x values is now governed by

$$\Delta p_x / p_F \approx -\hbar\omega / E_F \lesssim 1 , \tag{9}$$

the minus sign indicating that only those levels for $E_m < E_F$ are allowed, neglecting $k_B T$. We therefore expect a kind of inhomogeneous broadening and consequently a shift of the observed resonance due to this p_x smearing. If we write our linear potential in the form $V(p_F) = (e/c) p_F H z/m$, then, for the lowest p_x value, we have $V(p_x) \simeq V(p_F)(1 - \hbar\omega/E_F)$. Such a softening of the potential forces the energy levels closer together; hence, the magnetic field at which the resonance is observed must be shifted upwards.

2. Large orbit

The skipping orbit in the high-frequency case no longer comprises a small segment—or "point"—of the total cyclotron orbit. With the higher fre-

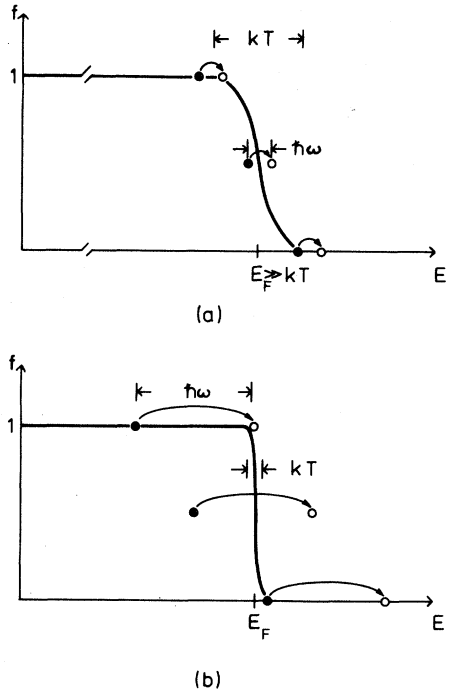

FIG. 2. Allowed transitions about the Fermi energy for (a) microwave frequencies and (b) far-infrared frequencies as applicable to Bi. f is the Fermi occupation function.

quencies, the resonances occur at higher magnetic fields [Eq. (5)], and the corresponding cyclotron radii become smaller. A formulation of the quantization condition,[5] equivalent to Eq. (1), is that the magnetic flux through the orbit be an integral number of flux quanta, with this number defining the energy-level number. Hence, as the field increases and the cyclotron radius decreases, one must increase the size of the skipping orbit relative to that of the cyclotron orbit in order to enclose the same number of flux quanta. The limiting situation is reached at cyclotron resonance itself, when the whole orbit encloses an integral number of quanta. Such a deviation of $(K/v_F^3)_1^{1/2}$ from its "point" value will give another contribution to the shift in the resonance when the orbit is noncircular.

3. Nonlinear potential

Along with the increasing size of the skipping orbit relative to the cyclotron orbit, a related effect of the high frequency becomes important. The Lorentz force is certainly no longer normal to the sample surface; the magnetic potential is therefore no longer linear, and the next-order quadratic term must be taken into account. The potential well becomes steeper, causing the energy levels to spread apart, thus leading to a shift of the observed resonance to lower fields.

4. Nonparabolic band effects

A final point, applicable in the case of Bi, is that nonparabolic band effects become important when the excitation energies become sufficiently large. In the following sections, we consider, in some detail, this and the above modifications to the microwave theory.

II. GENERALIZED SEMICLASSICAL CALCULATION

Emboldened by the success of the simple semiclassical approach in calculating the energy levels for the microwave surface states, we now generalize this approach to include the high-frequency effects described above. We treat first the case of a parabolic band structure, and indicate at the end of this section how the results are modified to include nonparabolicity. Our generalized quantization closely parallels that of Kaner, Makarov, and Fuks.[6]

A. Generalized energy levels

We consider the quadratic dispersion relation

$$E(p_x, p_z) = \frac{p_x^2}{2m_1} + \frac{p_z^2}{2m_3} \tag{10}$$

appropriate for a cylindrical Fermi surface. The magnetic field H is along the cylinder axis y, and the z direction points into the sample surface.

The vector potential in the Landau gauge is therefore given by

$$\vec{A} = (Hz, 0, 0). \tag{11}$$

Making the replacement $p_x \to p_x + (eH/c)z$ $(e>0)$, one obtains for the total energy

$$E = \frac{p_z^2}{2m_3} + \frac{1}{2m_1}\left(p_x + \frac{eH}{c}z\right)^2 + V(z), \tag{12}$$

where we have explicitly included the surface potential

$$V(z) = 0, \quad z > 0,$$

$$V(z) = \infty, \quad z < 0.$$

The electron is thus bound in the z direction by the effective potential

$$V_{eff} = \frac{1}{2m_1}\left(p_x + \frac{eH}{c}z\right)^2 + V(z), \tag{13}$$

and undergoes subsequent periodic motion in this direction. The orbit center z_0, defined by $V_{eff} - V(z) = 0$, is given by

$$z_0 = -cp_x/eH. \tag{14}$$

We assume for the moment $p_x \geq 0$, that is, we treat only orbits smaller or equal to a half cyclotron orbit; the results are easily extended to include the more general case.

The maximum penetration depth z_n of the electron occurs at the classical turning point $V_{eff}(z_n) = E_n$. E_n is the energy of the nth quantum level, and we take the zero of energy at $V_{eff} = 0$. We have therefore

$$z_n = (c/eH)[-p_x + (2m_1E_n)^{1/2}]. \tag{15}$$

Application of the quantization rule

$$2\int_0^{z_n} p_z\,dz = (n - \tfrac{1}{4})h, \quad n = 1, 2, \ldots, \tag{16}$$

together with the use of Eqs. (12) and (15), yields an implicit solution for the energy levels:

$$(n - \tfrac{1}{4})h = \frac{2c}{eH}(m_1m_3)^{1/2}E_n\left[\arcsin\left(1 - \frac{p_x^2}{2m_1E_n}\right)^{1/2} - \left(1 - \frac{p_x^2}{2m_1E_n}\right)^{1/2}\left(\frac{p_x^2}{2m_1E_n}\right)^{1/2}\right]. \tag{17}$$

As a check on this expression we consider two limiting cases.

1. Orbit center at the surface

Setting $p_x = 0$ in Eq. (17) gives the well-known result

$$E_n = \hbar\omega_c(2n - \tfrac{1}{2}) \tag{18}$$

where $\omega_c = (eH/c)(m_1m_3)^{-1/2}$. That is, the energy levels are spaced at twice the cyclotron frequency.

2. Prange-Nee limit—grazing incidence

We divide the total energy E_n into its contributions from motion parallel and normal to the sample surface,

$$E_n = (p_x^2/2m_1) + E_z(n) . \tag{19}$$

For grazing incidence, one has

$$p_x^2/2m_1 \gg E_z(n) , \tag{20}$$

yielding the usual microwave surface-state result,

$$E_z(n) = (2m_3)^{-1/3}(e\hbar p_x/m_1 c)^{2/3} H^{2/3} \times [\tfrac{3}{2}\pi(n-\tfrac{1}{4})]^{2/3} . \tag{21}$$

In Fig. 3 is depicted the energy-level scheme of Eq. (17) in the high- and low-frequency limits as a function of p_x (i.e., orbit center) for fixed magnetic field.

B. Calculation of resonance fields

Experimentally, the frequency ω is held fixed and the field H is varied. We therefore wish to find those fields H_{mn} for which the resonance condition $E_n - E_m = \hbar\omega$ is satisfied. Additionally, we will require that the maximum energy of the lower state E_m and the minimum energy of the upper state E_n coincide with the Fermi energy E_F (see Fig. 3). This requirement defines an allowed range of p_x values and a spread in the solutions for H_{mn}. From Eqs. (17) and (4), we obtain the coupled set of equations

$$H_{mn} = \frac{2c}{eh}(m_1 m_3)^{1/2} \frac{E_n}{n-\frac{1}{4}} \left[\arcsin\left(1 - \frac{p_x^2}{2m_1 E_n}\right)^{1/2} - \left(1 - \frac{p_x^2}{2m_1 E_n}\right)^{1/2}\left(\frac{p_x^2}{2m_1 E_n}\right)^{1/2}\right], \tag{22}$$

$$H_{mn} = \frac{2c}{eh}(m_1 m_3)^{1/2} \frac{E_n - \hbar\omega}{m-\frac{1}{4}} \times \left[\arcsin\left(1 - \frac{p_x^2}{2m_1(E_n-\hbar\omega)}\right)^{1/2} - \left(1 - \frac{p_x^2}{2m_1(E_n-\hbar\omega)}\right)^{1/2}\left(\frac{p_x^2}{2m_1(E_n-\hbar\omega)}\right)^{1/2}\right] .$$

Solving these equations numerically for the condition $E_n = E_F$ yields a value H_{mn}^- for the resonance field and a value $p_x^-(m, n)$ for the parallel momentum. Similarly, one obtains H_{mn}^+ and $p_x^+(m, n)$ for the condition $E_n = E_F + \hbar\omega$.

Assuming that all transitions between the limiting fields H_{mn}^+ and H_{mn}^- occur with equal weighting, we can write the expected resonance field

$$\bar{H}_{mn} = \tfrac{1}{2}(H_{mn}^+ + H_{mn}^-) . \tag{23}$$

The halfwidth of the resonance due to p_x broadening can be estimated by

$$\Delta H/H \sim |H_{mn}^+ - H_{mn}^-| / \bar{H}_{mn} . \tag{24}$$

We summarize briefly at this point by remarking that, besides including the effect of p_x broadening into our model, we have automatically also included the effect of the nonlinear magnetic potential and have exactly treated the elliptical orbits applicable to Bi. We shall now consider the last of the high-frequency effects listed in the Introduction.

C. Nonparabolic effects

Although we have assumed a parabolic band in Eq. (10), it is well known that the band structure in Bi is quite nonparabolic because of coupling between the valence and conduction bands. Nonparabolicity has a strong influence on the Azbel'-Kaner cyclotron resonance (AKCR) spectrum in the far infrared, [7] and we must therefore also expect a non-negligible effect on the surface-Landau-level spectra in this frequency regime.

The energy levels E_n' in the ellipsoidal nonparabolic (ENP) model[8] of the Bi band structure are given by

$$E_n'(1 + E_n'/E_G) = E_n + \hbar^2 k_H^2/2m_2 \pm \tfrac{1}{2} g\mu_B H . \tag{25}$$

Here, E_G is the energy of the gap which separates the valence and conduction bands. The k_H term represents the subband energy variation along the magnetic field, and the last term is the spin-splitting factor, where μ_B is the Bohr magneton. We continue for the moment to ignore k_H and spin effects. All masses appearing in this equation are those at the bottom of the conduction band.

For the ordinary bulk Landau levels, the level energy is simply $E_n = (n-\frac{1}{2})\hbar\omega_c$. To apply Eq. (25) to the surface Landau levels, we need only make the replacement

$$E_n \to E_n'(1 + E_n'/E_G) \tag{26}$$

in Eqs. (17), (4), and (22). For $E_G \to \infty$, of course, we recover the parabolic results.

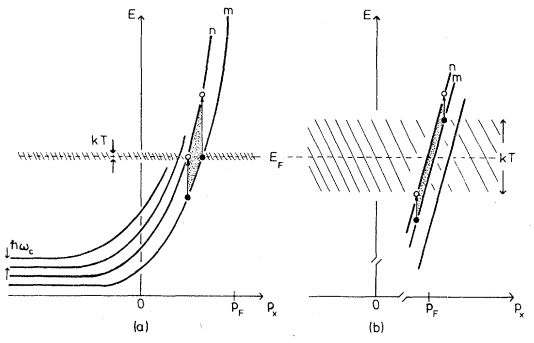

FIG. 3. Dependence of energy levels on p_x (orbit center) for a constant magnetic field. In the far infrared in Bi (a), the allowed transitions have unequal spacing ($\sim\hbar\omega$). so that at constant frequency the resonances are broadened and shifted in field position. In the microwave case (b) the allowed transitions have constant spacing.

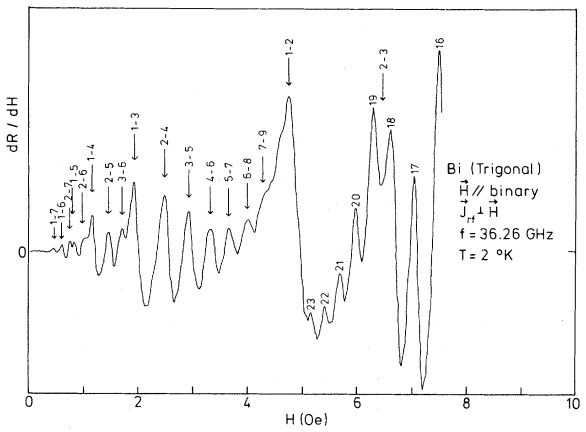

FIG. 4. Microwave surface-Landau-level resonances in Bi. The transitions are identified as $m \rightarrow n$. On the high-field end, the AKCR resonances are labeled by their Δn values.

III. EXPERIMENTAL NOTES

The high-frequency spectrometer system used in these studies has been well described elsewhere.[7,9] We will therefore only briefly relate those features essential to a general description of the experiment.

The far-infrared radiation was provided by a cw gas laser operated at four selected frequencies: 890.7, 1362.5, 1747.1, and 2526.6 GHz. The radiation is guided through a brass light pipe and condensing cone into a TEM mode strip transmission line in the cryostat. The transmission line consists of two parallel plates (~ 25-μm separation), one of which is the sample, the other a polished copper plate. For such a transmission line, the currents $\vec{J}$ induced in the plates flow along the transmission direction. A superconducting Helmholtz pair provides the magnetic field in the configuration $\vec{J} \perp \vec{H}$. The field is modulated at a frequency (~ 10 Hz) compatible with the detector time constant.

The power transmitted through the transmission line is detected by a Ga-doped Ge bolometer, placed well away from the magnetic field, near the bottom of the cryostat. Since the fractional power change $\Delta P/P$ due to resonant surface-Landau-level absorption is small, the detected signal is a measure of dR/dH, the field derivative of the surface resistance.

The Bi sample used in these studies is a trigonal plane sample whose size is $11 \times 40 \times 3$ mm^3. The long axis of the sample, along the transmission-line $\vec{J}$ direction, is parallel to the crystallographic bisectrix asis; the field H is thus along the binary axis in the sample plane. This sample, also used in a previous work,[7] was chemically polished in a solution consisting of six parts HNO_3, six parts CH_3COOH, and one part H_2O.

IV. RESULTS

In presenting our high-frequency surface-state data, we wish first to make some general observations concerning the appearance of the spectra and the identification of particular transitions. We will then take a close look at how these spectra evolve and scale in field position with increasing frequency in the infrared regime. For both the identification of transitions and the frequency scaling we will make use of the calculations resulting from the semiclassical analysis of Sec. II.

A. General observations

To provide an experimental frame of reference for the infrared surface-state system, we show in Fig. 4 a particularly beautiful surface-state spectrum in Bi taken in the more familar microwave regime. At the lower end of the trace we see a fairly large number of surface-state transitions, and at the high end we see AKCR harmonics. The transitions as marked can be directly compared with Eq. (5); thus the field positions measure the parameter $(K/v_F^3)_\perp^{1/2}$.[4] The overlap integrals for wave functions and rf field (penetration δ) are largest for transitions from the ground state (to put it a bit more crudely, $z_1 \sim \delta$), so that such transitions dominate the spectrum for each group of constant $(n-m)$ peaks. Line shapes for the resonances at microwave frequencies have been calculated,[10] and can be directly compared to the experimental traces.[2,4] In the microwave regime, therefore, peak positions, widths, and amplitudes are well understood. In Fig. 5 is indicated the location on the Bi Fermi surface of the resonant electrons corresponding to the trace of Fig. 4. The surface-state electrons skip about the $v_z = 0$ line on a cyclotron orbit segment of about 10° as viewed from the ellipsoid center.

We turn now to the surface-state spectrum at the lowest of our available far-infrared frequencies. Figures 6 and 7 show the resonances at 891 GHz,

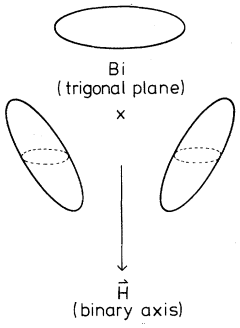

FIG. 5. Schematic slice of the Bi-electron Fermi surface in the trigonal plane. For a magnetic field along the binary axis, the central cyclotron orbits on the equivalent ellipsoids are dashed in. The relevant skipping orbits are fractions of these cyclotron orbits.

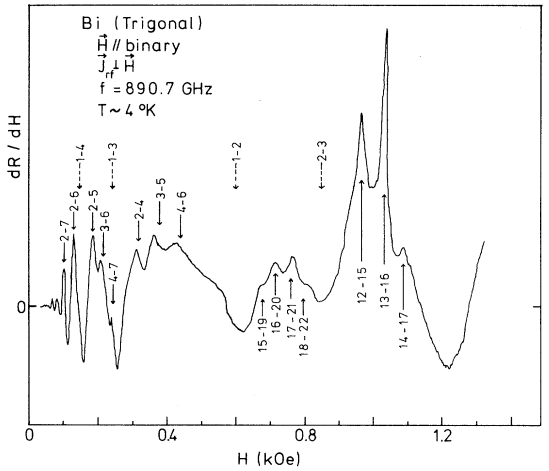

FIG. 6. Surface-Landau-level resonance at 891 GHz. The transitions are marked by their $m \rightarrow n$ values. Missing transitions from the lowest Landau level are indicated by dashed arrows. The upward arrows mark the $\Delta n = 3$ and $\Delta n = 4$ AKCR transitions (Ref. 7).

which is a factor of 25 higher than the microwave frequency of Fig. 4. The peak positions are marked according to the calculation outlined in Sec. II, and we comment below in more detail concerning this procedure. To reassure the reader who does not yet quite trust the calculation at this point, we remark that at 891 GHz the marking procedure does not critically determine transition identification; even the simple $\omega^{3/2}$ scaling of Eq. (5) yields field values which differ by only a few percent from the marked values. The amplitude decay of the low-field peaks in Fig. 6 is artificial, and is due to overmodulation of the magnetic field; Fig. 7 shows the detail of the low-field region with proper field modulation.

The surface-state spectrum in the far infrared bears a curious resemblance to a series of AKCR subharmonics, and it is tempting to try to interpret the spectra as a kind of incomplete-orbit cyclotron resonance. The orbits are, after all, no longer small fractions of a cyclotron orbit, and for half orbits one does expect a harmonic series [Eq. (18)]. We note, however, that the harmonic numbers for the peaks obtained by such an assignation must correspond to the difference Δn between Landau-level quantum numbers. But these differences do not agree with the $(n - m)$ values for the marked surface-Landau-level transitions; in Figs. 6 and 7, the $2 \rightarrow 6$ transition, for example, would be assigned on the basis of periodicity, the "AKCR" subharmonic number $\Delta n = 3$, whereas in reality $n - m = 4$. An examination of the surface-state level scheme [Eq. (5)] shows that, in general, transitions from a specific Landau level follow approximately such a pattern for $n - m > 3$.

Comparison of the 891-GHz spectrum with the microwave spectrum of Fig. 4 reveals some rather striking differences. First, there is a complete absence of transitions from the lowest Landau level at the high frequency. These are the transitions which dominate the spectrum at microwave frequencies! Second, the observed resonances are rather broad, far broader than expected from a naive scaling of $\omega\tau$ from the microwave frequency, and somewhat broader than the AKCR peaks seen also in Fig. 6. As we observed above, one expects the "p_x broadening" to play an important role in the infrared. We postpone a detailed discussion of these points until we have examined the data at three higher far-infrared frequencies.

B. Peak positions in the far-infrared

Spectra similar to that seen at 891 GHz are observed at three higher frequencies in the far-infrared regime (Figs. 8, 9, and 10). In this section we wish to examine the details of determining the peak positions as marked in the figures.

The basic idea behind our method of predicting the far-infrared peak positions is to carefully fit the necessary parameters to the microwave peak positions and then ask for the frequency evolution of the resonance fields. At 36.26 GHz, the $1 \rightarrow 2$ transition is observed[11] at 4.76 Oe (Fig. 4). The ordinary Prange-Nee scaling is, of course, simply $\omega^{3/2}$ [Eq. (5)]. In order to separate the effects involved in deviation from the $\omega^{3/2}$ scaling, we consider the calculation of Sec. II for both the parabolic and nonparabolic band models.

To obtain the parameters for the parabolic band, we use Eq. (21) to write the resonance field at microwave frequencies in the form

$$H_{mn} = \left(\frac{c^2\hbar}{e^2}\right)^{1/2} \left(\frac{\omega}{a_n - a_m}\right)^{3/2} \left(\frac{m_1 m_3}{E_F}\right)^{1/2} . \qquad (27)$$

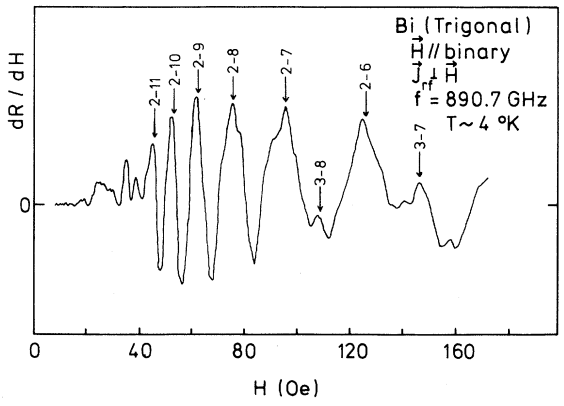

FIG. 7. Low-field detail of the 891-GHz spectrum.

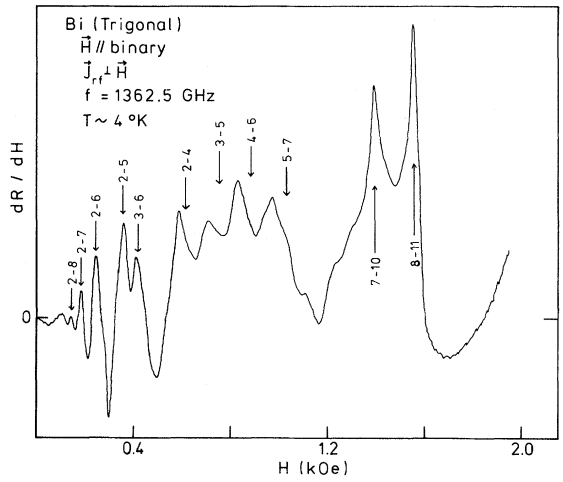

FIG. 8. Surface-Landau-level resonance at 1362 GHz. The transitions as marked are those predicted by the semiclassical calculation. The upward arrows mark the $\Delta n = 3$ AKCR transitions (Ref. 7).

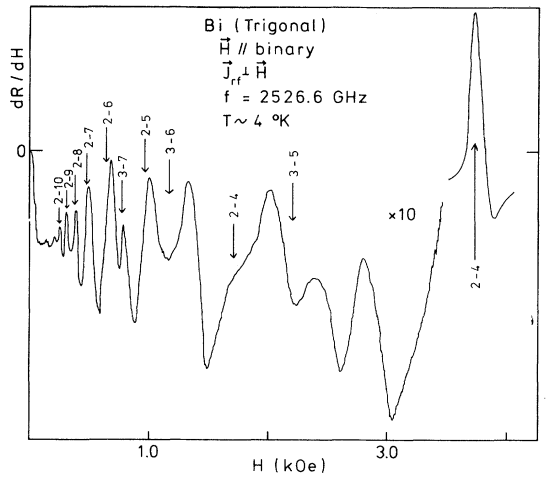

FIG. 10. Surface-Landau-level resonance at 2527 GHz. The transitions as marked are those predicted by the semiclassical calculation. A $\Delta n = 2$ AKCR resonance (Ref. 7) is marked just below 4 kOe.

[This is equivalent to Eq. (5).] The factor $(m_1 m_3)^{1/2}$ is, for our geometry, simply the cyclotron mass in the binary direction, and has the measured value[12] $m_c^*(E_F) = (0.0093 \pm 0.0001) m_0$, in excellent agreement with the value for the AKCR resonances of Fig. 4. The Fermi energy in this model is now fixed through Eq. (27) by our microwave results: $E_F = 17.9$ meV. Application of Eqs. (22) and (23) yields the predicted peak positions for the parabolic model at the desired frequencies.

For the nonparabolic model we need the Fermi energy, the gap energy, and the cyclotron mass at the bottom of the conduction band. This mass is related to the value used above by

$$m_c^* = m_c^*(E_F)(1 + 2E_F/E_G)^{-1}. \tag{28}$$

For the Fermi energy, we use the value measured in Ref. 7, $E_F = 29.8 \pm 0.6$ meV above the bottom of the band. We now perform the calculation required by Eqs. (22) and (26) for the microwave case, adjusting E_G to give agreement with the observed resonance fields. We find $E_G = 15 \pm 2$ meV. With these values for the band parameter, we can now go on and compute the infrared peak positions. The results for $\bar{H}_{mn}$ [Eq. (23)] are summarized in Table I.

A brief word concerning the accuracy of the results is in order. Since the infrared peak-position predictions are referred to the observed microwave resonance field, it is the accuracy of this field which for the most part determines the error limits of the predicted fields within each model. Experimentally, we determine the peak position for a trace such as Fig. 4 to an accuracy of about $\pm 1\%$.[2,4] Following the treatment of Refs. 2 and 4 for $\omega\tau \sim 20$, we have additionally assumed that the peak occurs at the resonance condition of Eq. (5), with the factor $(a_2 - a_1)^{-3/2}$ equal to the Prange-Nee value 0.432. This assumption introduces an additional uncertainty of about $\pm 1.5\%$, so that in summary we must consider the microwave result to which we are fitting and the subsequent scaling prediction to have an inherent uncertainty of about $\pm 2.5\%$. For the well-resolved peaks of the far-infrared spectrum we judge the uncertainty in the measured field position to be about $\pm 1.5\%$; thus, for a successful scaling theory, we require agree-

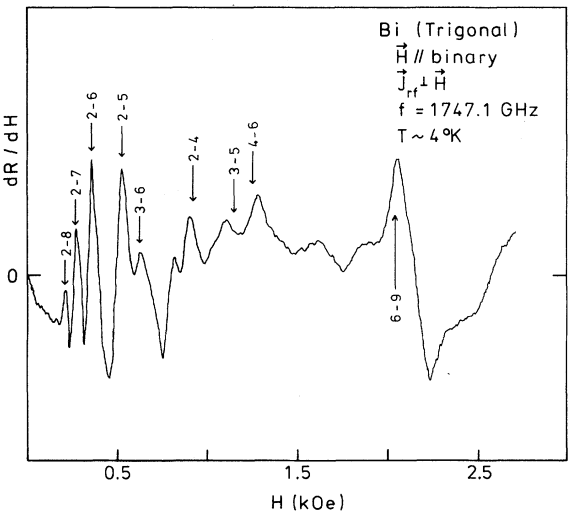

FIG. 9. Surface-Landau-level resonance at 1747 GHz. The transitions as marked are predicted by the semiclassical calculation. Near 2 kOe, a single AKCR transition is marked.

TABLE I. Experimental and calculated field positions for the best resolved far-infrared surface-Landau-level resonances. The experimental values are accurate to about ±1.5% and the calculated values to about ±2.5%. The calculations are labeled as PN ($\omega^{3/2}$ scaling), PB (parabolic band model), and NPB (nonparabolic band model). The last column gives the average deviation of the listed peaks for each model from the experimental values.

		H_{mn} (Oe)									
	$m \rightarrow n$	2–5	3–6	2–6	3–7	2–7	2–8	2–9	2–10	2–11	Average deviation (%)
Frequency (GHz)											
890.7	Expt	181	206	125	145	95	75	63	54	47	
	PN	177	205	122	139	92	73	61	52	45	3.0
	PB	184	216	127	146	95	76	63	53	46	1.6
	NPB	183	214	126	145	95	75	62	53	46	1.3
1362.5	Expt	358	410	246	···	179	145				
	PN	335	388	231	264	174	139				5.8
	PB	359	425	246	285	184	147				1.6
	NPB	354	418	242	281	182	145				1.3
1747.1	Expt	522	619	358	···	269	209				
	PN	486	564	335	383	253	202				6.3
	PB	538	644	366	429	274	218				3.2
	NPB	523	623	357	416	267	212				0.7
2526.6	Expt	1000	1305	667	775	493	384				
	PN	845	980	583	666	440	351				14.4
	PB	1030	1240	689	836	511	404				4.7
	NPB[a]	961	1170	644	771	479	379				3.7

[a]Spin shift included.

ment between prediction and measurement of about ±4%.

Examination of Table I reveals that the nonparabolic band calculation is able to account for the observed field values at all four far-infrared frequencies. In general, these observed values rise faster with frequency than the $\omega^{3/2}$ scaling would suggest; at the higher three frequencies, the deviation of observed fields from $\omega^{3/2}$ scaling becomes significant. The parabolic calculation overcorrects this deviation, and it is necessary to take band nonparabolicity into account to reduce the upward shift. The tendency toward a net upward shift in peak position is suggested by a perturbation calculation[13] of the "p_x shift" and "nonlinear potential shift," which were qualitatively discussed in the Introduction. The p_x shift toward higher field is larger than the nonlinear potential shift toward lower field, giving a net positive shift in field position.

There is considerable deviation from the nonparabolic prediction for the transitions at the highest fields in Fig. 10. We suggest as a possible cause the failure of Eq. (23), which we have used in calculating the resonance fields. This relation assumes that all transitions within the allowed p_x spread contribute equally to a resonance. At 2527 GHz, however, we are approaching the "cyclotron limit," i.e., some high-field surface-state transitions correspond to electrons which are nearly completing a full cyclotron orbit before collision with the surface. The resulting resonance fields are therefore not too far from the corresponding AKCR resonances—witness the 2→4 transition in Fig. 10. Since the AKCR resonance field is independent of p_x [Fig. 3(a)], one might expect a tendency for the surface-state resonance to be shifted toward the AKCR field because there are more allowed transitions per unit p_x at the high-field end. A further word of caution relevant to the cyclotron limit is that in this regime a transition must occur from phase factor $\frac{1}{4}$ [Eq. (16)], valid for the surface levels, to the usual factor $\frac{1}{2}$, which applies to volume-Landau levels; in this transition regime, our calculated fields cannot be correct.

V. DISCUSSION

The good agreement between the experimental fields and those calculated with nonparabolic band effects suggests that we have included the major mechanisms which cause deviation from the $\omega^{3/2}$ scaling law valid in the microwave regime. Although complete confirmation of the ideas presented here can come only with an extension of the Prange-Nee surface-impedance calculation[1,10] taking into

account the far-infrared effects in Bi, one can nevertheless estimate the influence of the far-infrared effects on the surface-state line shapes. It is this influence which we wish to discuss in this section.

A. Transition probabilities

Turning our attention first to the lack of observable transitions from the lowest bound state—those transitions which are most prominent at microwave frequencies—we are led to examine the inherent probabilities of transitions between the various quantum levels for clues.

Consider the matrix elements for the transitions. They are of the form $\langle\varphi_n|\mathcal{E}(z)|\varphi_m\rangle$,[1] where $\mathcal{E}(z)$ is the rf electric field as a function of distance z into the metal, and the φ_n are the z-dependent parts of the electronic wave function. (The φ_n are Airy functions in the Prange-Nee limit,[1] but are the more complicated parabolic cylinder functions in our more general case.[14]) As an illustration, we take $\mathcal{E}(z)=\mathcal{E}(0)e^{-z/\delta}$, where δ is the skin depth. For $z\ll\delta$, we approximate the exponential by $1-z/\delta$, so that the matrix element reduces to $\langle\varphi_n|z/\delta|\varphi_m\rangle$, the constant term vanishing by orthogonality. We therefore expect the transition probability in this case to vary as something like $(z_m/\delta)^2$. For $z\gg\delta$ the transition probability vanishes because of the exponential decay of the rf field. Our largest transition amplitudes should be found for those transitions where $z_m\sim\delta$. This qualitative picture is borne out in the detailed lineshape calculations[10] applicable in the microwave regime.

Using Eq. (15) with p_x values from Eq. (22), we obtain the skipping depth z_m at the various frequencies. To estimate the skin depth δ, we use the ratio R/δ (R is the cyclotron radius at the fundamental AKCR resonance) found as a function of frequency in the far infrared by Strom, Kamgar, and Koch.[7] The results are summarized for a few important transitions in Table II. The trend in the infrared toward suppression of transitions from the ground state is apparent.

B. Linewidths

At microwave frequencies, the linewidth of a surface-state resonance is a measure of the scattering rate $1/\tau$ of the resonant electron on the Fermi surface through the linewidth parameter $\omega\tau$. When τ is not itself a function of frequency, the linewidth varies as $1/\omega$, and in the infrared one would expect to see resonances orders of magnitude narrower than in the microwave regime. That this is not the case is immediately apparent upon comparison of Figs. 4, 6, and 7. Studies of AKCR[7] and of the dielectric anomaly[15] show that τ is in fact quite strongly frequency dependent; the AKCR resonances have linewidth $\Delta H/H$ at least an order of magnitude larger than the 0.13% value expected for frequency independent τ. The surface-state resonances we observe are nearly another order of magnitude broader than the AKCR resonances. We expect the p_x broadening to contribute substantially to the observed linewidths. Let us examine this possibility on the basis of the numbers.

The observed linewidths in the infrared range from about 10% at 891 GHz to about 15% at 2527 GHz, and do not depend strongly on field. Using Eq. (24) to estimate the linewidths, we find for the parabolic band case that the widths are also essentially field independent, but increase roughly linearly with frequency from about 10% to 891 GHz to 40% at 2527 GHz. These widths are radically altered by the inclusion of nonparabolicity. The nonlinearity of the relation given by Eq. (26) causes a considerable energy-dependent distortion of the $E_n(p_x)$ curves of Fig. 3(a) leading to a narrowing of the lines. (This distortion is severe enough to cause H^-_{mn} to be smaller than H^+_{mn}, contrary to the parabolic case.) One now finds $\Delta H/H$ values ranging from about 4% at 891 GHz to 8% at 2527 GHz.

An improvement of the width estimation is provided by taking the spin term of Eq. (25) into account with[16] $g\approx 2(m_0/m_c^*)$. The effect of the spin

TABLE II. Approximate ratios of electron penetration z_n to rf skin depth δ. The z_n values are calculated at the resonance field for each transition.

f (GHz)		36	891	1362	1747	2527
δ (10^{-5} cm)		9[a]	4.0[b]	3.8[b]	3.6[b]	3.1[b]
$m\rightarrow n$						
1–2	z_m/δ	0.5	0.2	0.2	0.2	0.2
	z_n/δ	0.9	0.4	0.4	0.3	0.3
1–3		0.7	0.3	0.3	0.3	0.3
		1.7	0.8	0.6	0.6	0.6
2–3		0.8	0.4	0.3	0.3	0.3
		1.1	0.5	0.4	0.4	0.4
2–4		1.2	0.5	0.5	0.4	0.4
		1.9	0.9	0.7	0.7	0.6
2–5		1.4	0.6	0.5	0.5	0.5
		2.7	1.2	1.1	1.0	0.9
2–6		1.6	0.7	0.6	0.6	0.6
		3.5	1.5	1.3	1.2	1.2
3–5		1.5	0.7	0.6	0.5	0.5
		2.1	1.0	0.8	0.8	0.7
3–6		1.8	0.8	0.7	0.7	0.6
		2.9	1.3	1.1	1.0	1.0

[a]This value for δ must be treated with some care. See Ref. 4.

[b]Estimated from Ref. 7.

term is easily calculated by using the result of the calculation without spin, $\overline{H}_{mn}$, to give a value for the spin term, and then iterating to convergence. One finds a substantial increase in linewidth and, at the highest frequency, a shift in peak position of about 2% due to the inhomogeneous nature of the p_x smearing and to the nonlinear energy scale from nonparabolicity. The width values $\Delta H/H$ obtained with inclusion of spin range from about 7% at 891 GHz to about 16% at 2527 GHz, reflecting well the experimental observations.

Inclusion of the k_H term in Eq. (25) is also expected to contribute to the linewidth. Judging from the microwave results,[2] we might expect an additional contribution of ~ 30% to the linewidth, but a nearly negligible effect on the peak position.

C. Surface scattering

It is at first glance remarkable that surface-Landau-level resonance is at all observable in the far infrared. At these frequencies, the skipping electrons are no longer reflected from the surface at glancing angles; on the contrary, resonances are observed for electrons specularly reflected at nearly normal angles of incidence on the surface. Since diffusive scattering effects from surface roughness are field and frequency dependent,[1,17] it is clear from the large range of frequencies over which we observe the surface states that surface roughness effects play little or no role.

This lack of observable surface scattering follows from the small size of the Bi Fermi surface and the consequently relatively long electron wavelength. Let us consider a real metal where, accidently[2] or deliberately,[17] surface roughness effects are observed at microwave frequencies. Here the glancing angle is typically of the order of 1°, and the parallel momentum k_F of order 10^8 cm^{-1}, so that normal to the surface we have $k_z \sim 10^6$ cm^{-1}. Appreciable surface roughness scattering occurs when $\lambda \sim 2\pi/k_z$ approaches the scale of surface roughness.[6] For typical experimental surfaces, therefore, one expects to observe surface scattering for $k_z \gtrsim 10^6$ cm^{-1}, a condition which is never reached in Bi.

VI. CONCLUDING REMARKS

On the basis of our far-infrared surface-state data in Bi, we have explored the corrections to the Prange-Nee theory which become important when the excitation energy $\hbar\omega$ approaches the Fermi energy E_F. Although these corrections will be relatively small in a real metal where E_F is far larger than in Bi, observation of surface-Landau-level resonance in such a metal is limited by the very stringent requirements of sample-surface preparation, which go hand in hand with the increasing Fermi wave vector k_F.

ACKNOWLEDGMENT

Finally, it is our pleasure to thank J. F. Koch for support, encouragement, and numerous stimulating discussions.

[1] R. E. Prange and T. W. Nee, Phys. Rev. 168, 779 (1968).

[2] The power of the method is best illustrated in Cu—see R. E. Doezema and J. F. Koch, Phys. Rev. B 5, 3866 (1972); 6, 2071 (1972).

[3] M. S. Khaikin, Zh. Eksp. Teor. Fiz. 55, 1696 (1968) [Sov. Phys.-JETP 28, 892 (1969)].

[4] J. F. Koch and J. D. Jensen, Phys. Rev. 184, 643 (1969).

[5] J. F. Koch, in *Solid State Physics*, edited by J. F. Cochran and R. R. Haering (Gordon and Breach, New York, 1968), Vol. I, Chap. X.

[6] E. A. Kaner, N. M. Makarov, and I. M. Fuks, Zh. Eksp. Teor. Fiz. 55, 931 (1968) [Sov. Phys.-JETP 28, 483 (1969)].

[7] U. Strom, A. Kamgar, and J. F. Koch, Phys. Rev. B 7, 2435 (1973).

[8] B. Lax and J. G. Mavroides, in *Advances in Solid State Physics*, edited by F. Seitz and D. Turnbull (Academic, New York, 1960), Vol. 11.

[9] M. Wanner, Diplom thesis (Technische Universität München 1974) (unpublished).

[10] T. W. Nee, J. F. Koch, and R. E. Prange, Phys. Rev. 174, 758 (1968).

[11] The value of the $1 \rightarrow 2$ peak position quoted here is about 4% higher than that expected from the work of Koch and Jensen (Ref. 4). This difference comes about because of a relatively strong shift of the peak position with $\omega\tau$ which is not satisfactorily explained by the theory. The error resulting from this shift is minimized when $\omega\tau$ is high as for the sample of Fig. 4. The velocity values of Ref. 4 obtained on samples with relatively low $\omega\tau$ are consequently too high by nearly 3%, and the cyclotron mass that is predicted by integration of the surface-state velocities is no longer in disagreement with the generally accepted AKCR value (Ref. 12).

[12] V. S. Edelman and M. S. Khaikin, Zh. Eksp. Teor. Fiz. 49, 107 (1965) [Sov. Phys.-JETP 22, 77 (1966)].

[13] U. Strom, Ph.D. thesis (University of Maryland, 1972) (unpublished).

[14] H. J. Fischbeck, Phys. Status Solidi B 45, 221 (1971).

[15] H. D. Drew and U. Strom, Phys. Rev. Lett. 25, 1955 (1970).

[16] G. E. Smith, G. A. Baraff, and J. M. Rowell, Phys. Rev. 135, A1118 (1964).

[17] J. F. Koch and T. E. Murray, Phys. Rev. 186, 722 (1969).